GpsB coordinates cell division and cell surface decoration by wall teichoic acids in *Staphylococcus aureus*

Lauren R. Hammond[1], Sebastian J. Khan[1], Michael D. Sacco[2], Catherine Spanoudis[1], Abigail Hough[1], Yu Chen[2] and Prahathees J. Eswara[1*]

[1] Department of Cell Biology, Microbiology and Molecular Biology, University of South Florida, Tampa, Florida, USA

[2] Department of Molecular Medicine, University of South Florida, Tampa, Florida, USA

[*]To whom correspondence should be addressed. Email: eswara@usf.edu

Keywords: GpsB; FtsZ; suppressors; cell division; cell wall; cell shape; WTA.

ABSTRACT

Bacterial cell division is a complex and highly regulated process requiring the coordination of many different proteins. Despite substantial work in model organisms, our understanding of the systems regulating cell division in non-canonical organisms, including critical human pathogens, is far from complete. One such organism is *Staphylococcus aureus*, a spherical bacterium that lacks known cell division regulatory proteins. Recent studies on GpsB, a protein conserved within the Firmicutes phylum, have provided insight into cell division regulation in *S. aureus* and other related organisms. It has been revealed that GpsB coordinates cell division and cell wall

synthesis in multiple species by interacting with Penicillin Binding Proteins (PBPs) and other partners. In *S. aureus*, we have previously shown that GpsB directly regulates FtsZ polymerization. In this study, using *Bacillus subtilis* as a tool, we isolated intragenic and extragenic spontaneous suppressor mutants that abrogate the lethality of *S. aureus* GpsB overproduction in *B. subtilis*. Through characterization of these mutants, we identified several key residues important for the function of GpsB. Furthermore, we discovered an additional role for GpsB in wall teichoic acid (WTA) biosynthesis in *S. aureus*. Specifically, we show that GpsB directly interacts with the wall teichoic acid export protein TarG using a bacterial two-hybrid analysis. We also identified a three-residue motif in GpsB that is crucial for this interaction. Based on the analysis of the localization of TagG in *B. subtilis* and its homolog TarG in *S. aureus*, it appears that WTA machinery is a part of the divisome complex. As such, we show additional evidence to the growing body of work that suggests that along with peptidoglycan synthesis, WTA biosynthesis and export may take place at the site of cell division. Taken together, this research illustrates how GpsB performs an essential function in *S. aureus* by directly linking the tightly regulated cell cycle processes of cell division and WTA-mediated cell surface decoration.

IMPORTANCE/AUTHOR SUMMARY

Cytokinesis in bacteria involves an intricate orchestration of several key cell division proteins and other factors involved in building a robust cell envelope. One of the key factors that differentiates Gram-positive bacteria from Gram-negative bacteria is the presence of teichoic acids interlaced within the Gram-positive cell wall. By

characterizing the role of *Staphylococcus aureus* GpsB, an essential cell division protein in this organism, we have uncovered an additional role for GpsB in wall teichoic acids (WTA) biosynthesis. We show that GpsB directly interacts with TarG of the WTA export complex. We also show this function of GpsB may be conserved in other GpsB homologs as GpsB and the WTA exporter complex follow similar localization patterns. It has been suggested that WTA acts as a molecular signal to control the activity of autolytic enzymes, especially during the separation of conjoined daughter cells. Thus, our results reveal that GpsB, in addition to playing a role in cell division, may also help coordinate WTA biogenesis.

INTRODUCTION

One of the defining characteristics of life is the ability for a cell to grow and divide. Although there are some exceptions, the predominate process for growth and division in bacteria is binary fission where one bacterial cell grows and divides to produce two similarly sized daughter cells [1, 2]. This tightly regulated process coordinates chromosome segregation, cell elongation, and controls the activity of cell division proteins [3, 4]. Although significant strides have been made to identify the molecular mechanism regulating the cell division machinery, gaps remain in our knowledge, particularly in the non-model organisms [2, 5]. For example, GpsB (the central protein of interest in this study) plays an important, and in some cases essential, role in the cell growth regulation of multiple clinically-relevant Gram-positive organisms (specifically Firmicutes), but is absent in Gram-negative organisms [6, 7]. This highlights the need for a closer analysis of such processes and proteins in multiple species.

In *Bacillus subtilis*, *Listeria monocytogenes* and *Streptococcus pneumoniae*, GpsB links cell wall biosynthesis with the cell division process by interacting with penicillin binding proteins (PBPs), thereby helping to regulate and maintain proper cell shapes [8-14]. Our lab reported that *S. aureus* GpsB directly interacts with FtsZ and affects its polymerization characteristics [15]. In our previous study, we described the lethal phenotype associated with the overproduction of *S. aureus* GpsB ($GpsB^{SA}$) in its Firmicutes relative *B. subtilis*. In this study, we utilized this phenotype to conduct a suppressor screen to identify residues that are important for the function of $GpsB^{SA}$ and pathways through which $GpsB^{SA}$ may exert its function. Herein, we describe the effects of seven intragenic $GpsB^{SA}$ suppressor mutations and characterize their ability to abrogate cell division inhibition. Additionally, we investigated extragenic suppressor mutations through whole genome sequencing that allowed us to delineate a novel role for GpsB in linking central cell division directly to the wall teichoic acids (WTA) pathway. Specifically, suppressor mutations were mapped to *tagG/tagH* genes in *B. subtilis*, and subsequent bacterial two-hybrid (BACTH) analysis confirmed the direct interaction between $GpsB^{SA}$ and the *S. aureus* homolog of TagG, TarG. We also show a 3-amino acid motif, positioned away from the well-characterized PBP binding site, that appears to be important for TarG binding. Furthermore, we show that the interaction between GpsB and the WTA export complex may be conserved beyond *S. aureus*, as we also note that TagH has similar spatiotemporal localization pattern as GpsB in *B. subtilis* cells. In *S. aureus*, treatment with antibiotics that target the WTA pathway drastically alters the localization pattern of GpsB, although targeting of GpsB to new division sites

remain unaffected. Thus, it appears that GpsB, an essential protein in *S. aureus*, coordinates cell division and WTA production/transport through direct interaction with FtsZ and TarG respectively.

RESULTS

Isolation of suppressor mutations of GpsB^{SA} overproduction in *B. subtilis*

To build upon our previous report and further explore other cell cycle processes that involve GpsB^{SA} in an unbiased manner, we isolated suppressors that can tolerate the lethal overproduction of GpsB^{SA} in *B. subtilis* [15]. Briefly, a *B. subtilis* strain harboring an IPTG-inducible *gpsB*^{SA}*-gfp* was streaked out on plates containing IPTG and incubated overnight. Following incubation, the colonies that appeared on the plates containing the inducer were presumed to contain spontaneous suppressor mutations. Non-GFP producing isolates were discarded, as the likely cause of the suppression of lethality could be a promoter mutation turning off the expression of *gpsB*^{SA}*-gfp*, a frameshift mutation, or a premature truncation. After multiple rounds of confirmatory screening, the mutations were classified to be either intragenic or extragenic (**Fig. 1A**) [16]. Using this method, we isolated seven intragenic mutations, Y14F, L35S, D41N, D41G, R72H, as well as a deletion and repeat of a 3-amino acid stretch 66-68 LEE (ΔLEE and LEErpt) that are listed in **Fig. 1B**, of these L35S was reported previously [15]. Throughout the manuscript, these suppressor mutations as a group will be referred to as *GpsB-GFP. We then analyzed the multiple sequence alignment of GpsB from *S. aureus*, *B. subtilis*, *L. monocytogenes*, and *S. pneumoniae* (**Fig. 1C**). Of the first four mutations (Y14F, L35S, D41N, and D41G), the latter three occur in highly conserved

residues. Tyr14 is wedged between a conserved Lys (Lys11) which was reported to be important for forming a bidentate salt bridge with the proximal glutamate/aspartate (Glu15 in *S. aureus*) in other organisms [6]. Of note, Phe replaces Tyr in the corresponding position (Tyr14 of *S. aureus*) in *S. pneumoniae* GpsB. The remaining three mutations (ΔLEE, LEErpt, and R72H) are near the disordered linker connecting the N- and C-terminal domains **(Fig. 1C**). The Leu, Glu, Glu (LEE) motif is conserved in *B. subtilis*, however Arg72 is less conserved but appears in *L. monocytogenes*.

Suppressor mutations of GpsB^{SA} abolish cell division inhibition in *B. subtilis* cells

To examine the ability of *B. subtilis* to tolerate the expression of **gpsB*^{SA}*-gfp*, we conducted a spot titer assay with a clean copy of *gpsB*^{SA}*-gfp* harboring the suppressor mutation cloned into PY79 cells under the control of an inducible promoter, similar to how the wildtype *gpsB*^{SA}*-gfp* was constructed. Cultures containing each of the strains were grown, serially diluted, and then plated onto LB agar plates both with and without inducer (**Fig. 2A**). On the minus inducer plate, all strains were able to grow and no growth defects were noted. On the plus inducer plate, the strain containing unmutated GpsB^{SA}-GFP showed a severe growth defect consistent with our previous report. In contrast, the growth on the minus and plus inducer plates for each of the suppressor mutations was indistinguishable from each other. Western blot analysis was used to confirm the stable production of each mutant in *B. subtilis* (**Fig. S1A)**. Although most suppressors are stably produced, L35S displayed a distinct cleavage product **(Fig. S1B)** and LEErpt appears to be more stable as it accumulates to a larger extent even in the

absence of the inducer. Regardless, all seven suppressor mutations in GpsB^{SA} allow *B. subtilis* cells to grow on solid medium in the presence of inducer.

We previously reported that the growth defect caused by the expression of *gpsB*^{SA} in *B. subtilis* was due to severe filamentation, which is characteristic of cell division inhibition in this organism [15]. To investigate the effect of the suppressor mutations on cell division inhibition, we performed high resolution fluorescence microscopy (**Fig. 2B**). Upon expression of *gpsB*^{SA}-*gfp*, we observed the previously reported cell division inhibition and filamentous phenotype (**Fig. 2B ix**). Notably, upon expression of each of the suppressor mutations, the *B. subtilis* cells no longer display the filamentous phenotype and appear to be dividing normally (**Fig. 2B x - xvi**). We also examined *GpsB-GFP localization in all strains (**Fig. S1C**). Diffused localization was observed for the L35S (as noted previously; [15]) and D41N suppressors (**Fig. S1C iii and v**). Otherwise, all *GpsB-GFP strains displayed a mostly wildtype-like localization pattern.

Most **gpsB*^{SA} mutants are dominant alleles and can suppress the toxicity of *gpsB*^{SA} upon co-expression

To determine if any of the **gpsB* mutations suppress the toxicity of the wildtype *gpsB*^{SA} allele, we engineered a *B. subtilis* strain to co-express both *gpsB*^{SA}-*gfp* and **gpsB*^{SA}-*gfp* under the control of an IPTG-inducible promoter to produce stoichiometrically equivalent amounts of both wildtype and mutant proteins. We then performed a spot titer assay to examine any growth defects in these strains (**Fig. S2A**). In the strains carrying the suppressor mutations, six were able to restore growth and grow both in the absence

and presence of inducer. The seventh mutation, Y14F, showed a weak dominant negative effect as it was able to grow in serial dilutions 2 to 3 log-fold higher than GpsB^{SA}-GFP alone. However, it was not as strong as the other mutations that grew in a serial dilution that was 5 to 6 log-fold higher than GpsB^{SA}-GFP. Interestingly cells overproducing Y14F variants are on average longer (3.92 µm, n=100) when compared to minus inducer control (2.18 µm, n=100) implying partial functionality of this mutant (compare Fig. 2B panels ii and x). Next, we used a BACTH assay to examine the protein-protein interactions that could explain this dominant negative effect. Since GpsB is known to form a hexamer (trimer of dimers), we tested the ability of each mutant to interact with WT GpsB^{SA} by cloning GpsB^{SA} and *GpsB^{SA} into the BACTH plasmids [17]. Pairs of these plasmids were transformed into BTH101 *Escherichia coli* cells for protein-protein interaction analysis on MacConkey agar and by β-galactosidase assay in liquid cultures (**Fig. S2B**). We found that all the mutants retained their ability to interact with WT GpsB. Thus, we believe that a GpsB^{SA}-*GpsB^{SA} interaction is likely the reason for the suppression in toxicity observed in **Fig. S2A**.

As GpsB is an essential protein in *S. aureus*, we wondered if the expression of these dominant suppressor mutation harboring copies of *gpsB* would impair the essential function of GpsB^{SA} in its native organism and be lethal to the cells. This straightforward analysis was complicated by the fact that overproduction of *gpsB-gfp* in *S. aureus* by itself is toxic and results in cell enlargement as reported previously [15]. Thus, we were not able to conduct a thorough analysis. However, among these suppressors it appears that Y14F, ΔLEE, and R72H are the most potent in inhibiting the function of native

GpsB, as colony formation is almost completely eliminated upon their overproduction (**Fig. S2C**). Stable production of *GpsB^{SA}-GFP in *S. aureus* cells was also confirmed through western blotting (**Fig. S2D**). Despite being one of the most toxic mutations, the ΔLEE mutant accumulates to a much lower extent than the other mutants.

Structural analysis of GpsB^{SA} suppressor mutations

The N-terminal domain of GpsB is characterized by an elongated coiled-coil dimer that is highly conserved among homologs (**Figs. 3 and S3**) and is highly similar to the lipid-binding domain of DivIVA [6]. The GpsB monomer has two regions of organized secondary structure: a long α-helix of approximately 35-40 residues (α-helix 2) and a shorter, two turn α-helix of approximately 8 residues (α-helix 1) (**Fig. 3A**). Near the membrane-binding region, α-helix 1 from one protomer converges at the interface of α-helix 2 and α-helix 1 from the other protomer to form a groove that binds to the cytoplasmic N-terminal domain of PBPs. Although the PBP binding site is conserved among GpsB homologs, a conclusive positive interaction between *S. aureus* GpsB and any of the PBPs has not been observed yet. The N-terminal domain of GpsB is connected by a non-conserved, disordered linker to a short, helical C-terminal domain.

Using the SWISS-MODEL homology-server, a homology model for the N-terminus of *S. aureus* GpsB was constructed, allowing us to predict the structural effects of these suppressor mutations (**Fig. 3**) [18]. The mutations described in our experiments likely disrupt the structural integrity of GpsB (L35S, D41N/D41G) or alter the recognition elements required for partner binding (Y14F, R72H, LEE repeat/deletion).

Tyr14 → Phe

Tyr14 is located on α-helix 1 near the PBP-binding groove where it is oriented outwards, away from the core and into the solvent accessible region (**Fig. 3B**). The aliphatic nature of the Tyr side chain is conserved in *S. pneumoniae*, *L. monocytogenes*, and *B. subtilis* where it is Phe, Leu, and Leu respectively. Using the structures of *L. monocytogenes*, *B. subtilis*, and S. *pneumoniae* GpsB complexed with their PBP binding partner (PDB IDs 6GPZ, 6GP7, and 6GQN, respectively), we observe that Tyr14 projects directly towards the PBP N-terminal helix [10, 14]. Because Tyr14 does not interact with other residues in GpsB and the Tyr → Phe mutation is relatively minor, a likely scenario for the more toxic phenotype (**Fig. S2C**), is that Tyr14 facilitates interaction with a binding partner. Furthermore, because the Tyr → Phe mutation corresponds to the loss of a phenolic hydroxyl group, the interaction likely involves the formation of a hydrogen bond.

Leu35 → Ser

Leu35 is positioned at the interface of the PBP binding site and the core of the coiled coil junction (**Fig. 3C**). Despite interacting with adjacent hydrophobic residues near the interfacial core, Leu35 is in immediate proximity to the canonical arginine that is required for PBP binding. However, a mutation to a more polar residue that is capable of hydrogen bonding would seemingly improve this interaction. Therefore, it is most likely that the L35S mutation disrupts the core hydrophobic interactions that are critical for maintaining either the overall structure, or the shape of the PBP binding groove. This

may explain the diffused localization (**Fig. S1**). Further supporting this hypothesis is an equivalent mutation at this position in *L. monocytogenes* GpsB, L36A that prevents oligomerization of GpsB, presumably due to the disruption of this hydrophobic core [10].

Asp41 → Asn, Gly

Asp41 is located on α-helix 2 where it interacts with a loop formed by the first 10 residues of GpsB that precedes α-helix 1 (**Figs. 3E, S3C**). Given the proximity of Asp41 to Lys7 and the fact that a mutation to the chemically similar, but neutral Asn produces a non-functional variant, one could mistakenly assume this is a critical electrostatic interaction. However, the side chain of Lys7 is 5.8 Å away from the closest Asp side chain oxygen, well beyond the expected range of favorable electrostatic interactions. Furthermore, Lys7 is not conserved amongst *L. monocytogenes* and *S. pneumoniae*; significantly, *S. pneumoniae* GpsB has an isoleucine at this position (**Fig. S3C**). A closer inspection of this region reveals that Asp41 is an important acceptor of three hydrogen bonds: from the strictly conserved Tyr42 of the adjacent protomer, and the amide nitrogen of the Lys7 and Leu8 main chain. The hydrogen bonds with the backbone nitrogen of Lys7 and Leu8 are important interactions because this attracts the loop to the helical core of GpsB, allowing α-helix 1 to interact with α-helix 2, thus correctly forming the PBP binding groove. Therefore, the replacement of any of the Asp oxygen atoms, even with a nitrogen hydrogen bond donor, would likely prohibit the formation of these three highly coordinated hydrogen bonds.

LEE deletion/repeat and Arg72 → His

The last two turns of the GpsB N-terminal α-helix 2 are composed of residues 66-LEELRLR-72. They are followed by a flexible linker region of approximately 20 amino acids that connects to the C-terminal domain. Interestingly, the LEELRLR region is not conserved amongst other Firmicutes and is unique to *S. aureus*. Multiple i +3 and i +4 electrostatic interactions are formed laterally along LEELRLR by Arg and Glu sidechains and Lys64 (**Figs. 3D, S4**). Additionally, the Leu residues interact through hydrophobic interactions in the core with the corresponding residue of the adjacent protomer and the neighboring Leu of its own chain. The insertion or deletion of a LEE sequence would disrupt the complementarity of sidechain interactions and cause charge-charge repulsion. Deletion of LEE eliminates a pair of (N+3/N+4) +/- interactions (K64-E67, E68) and (E68-R72) while adding one pair of +/+ interactions (K63, K64 -E67R) (**Fig. S4C**). A LEE repeat eliminates one +/- interaction (E68-R72) and adds two pairs of -/- interactions: (E67-R70E, L71E) and (E68- L71E, R72E) (**Fig. S4B**). Therefore, the insertion or deletion of LEE will decrease the helical propensity of this region. Because the disruption of secondary structure is restricted to a small region that is adjacent to a disordered linker, the impact on the overall structure of GpsB structure could be minimal, meaning this specific area may have functional importance for binding to other proteins. Possible proteins include FtsZ [15] or other unique interaction partners (such as TarG discussed later in this report) that could interact with GpsB through LEELRLR. Additionally, Arg72 is either the last residue of α-helix 2 or the beginning of the disordered, linker region that connects the N-terminal domain to the C-terminal domain. Either way, it is unlikely to affect the overall structure of GpsB and could also be a

critical residue that interacts with another protein, likely through electrostatic interactions with a Glu or Asp residue.

Isolation of extragenic suppressors reveals a link between GpsB and wall teichoic acid machinery

In addition to the intragenic suppressors described above, we also isolated extragenic suppressors and then analyzed these mutants through whole genome sequencing (**Fig. 1A**). Through this process we isolated three different suppressor mutations independently. Two of the mutants had the same mutation in *tagH* (Y233C) and the third suppressor had a mutation in *tagG* (R20K) (**Fig. 4A**). TagG and TagH work together to form a complex that exports wall teichoic acids (WTA) that are made intracellularly so they can be anchored to the cell wall [19]. As these WTA genes are essential in *B. subtilis*, to confirm that the extragenic suppressors harbor true suppressor mutations we utilized the previously developed essential gene knockdown tool based on CRISPR interference (CRISPRi) with deactivated Cas9 [20], to disrupt the expression of either *tagG* or *tagH*. Briefly, we investigated the fate of wildtype GpsB^{SA}-GFP overproducing cells when *tagG* or *tagH* expression was knocked down (+ xylose) or not (**Fig. 4C**). When we imaged these *tagG* or *tagH* strains without xylose (**Fig. 4B i and iii)**, the strains appeared similar to wildtype. Upon addition of xylose, we noted areas of membrane enrichment near cell poles (**Fig. 4B ii and iv)**, consistent with the previous report of bulging [20]. As shown before (**Fig. 2B)**, induction of *gpsB^{SA}-gfp* expression with IPTG leads to filamentation (**Fig. 4C i and ii,**). In the CRISPRi strains of *tagG* or *tagH* with GpsB^{SA}-GFP, the IPTG-mediated filamentation is also seen in the

absence of xylose (no interference in the expression of *tagG* or *tagH*) (**Fig. 4C iv and viii**). Finally, when we add both IPTG and xylose to induce GpsB^{SA}-GFP production and knockdown of *tagG* or *tagH*, the cells are no longer filamentous (**Fig. 4C vi and x**), thus confirming that *tagG* and *tagH* are true suppressors of GpsB^{SA}-GFP mediated cell division inhibition. Therefore, it is likely that the extragenic suppressor mutations result in dysregulation of the TagGH complex to suppress the lethal overexpression of *gpsB^{SA}*.

To our knowledge, a direct relationship of GpsB and WTA synthesis has not been reported in *B. subtilis*. So, to investigate how TagGH could suppress GpsB^{SA}-GFP mediated cell division inhibition, we monitored both GpsB and TagGH localization in *B. subtilis* cells. Using GpsB^{BS}-GFP and GFP-TagH^{BS} [21], we analyzed when TagH arrived at the division site (**Fig. 4D**). We found that both GpsB^{BS} and TagH^{BS} arrives at mid-cell early in the division cycle, (at a similar time to GpsB^{SA} in *B. subtilis* [15]), in areas of membrane enrichment (indicating the regions of septal membrane invagination) (**Fig. 4D i and iv; see arrowhead**) and stays at the mature septum (**Fig. 4D ii and v**), at least until the septum transforms into hemispherical cell poles (**Fig. 4D iii and vi)**. This is consistent with the previous reports of TagH^{BS} [21] and GpsB^{BS} localization [8, 9]. Thus, it appears that GpsB may play a role in WTA biosynthesis by interacting with one or more of the WTA biosynthesis proteins, and the toxicity stemming from GpsB^{SA} production in *B. subtilis* could be due to an interaction between GpsB^{SA} and the TagGH^{BS} WTA exporter complex.

GpsB^{SA} directly interacts with *S. aureus* wall teichoic acid export protein TarG

Next, we analyzed whether GpsB^{SA} could interact directly with the *S. aureus* homologs of TagGH, TarGH (Tag - teichoic acid glycerol | Tar - teichoic acid ribitol; [19]), using a BACTH assay. We detected a strong positive interaction between TarG^{SA} and GpsB^{SA} (**Fig. 5A**). We further confirmed the strong positive interaction by quantifying the production of β-galactosidase enzyme **(Fig S5A)**. Interestingly, a previous work has showed an interaction between GpsB^{SA} and TarO^{SA} via BACTH [22].

Since we could detect an interaction between GpsB and the WTA export complex, we were curious if overexpression of *gpsB* would affect WTA levels in *S. aureus* cells. Crude WTA extracts from *S. aureus* cells containing either an empty vector or one overproducing GpsB were visualized under Alcian blue silver staining, but we did not detect any changes in WTA levels in these cells at the condition tested (**Fig. S5B**). In addition, we also observed early division site localization of GFP-TarG (**Fig. S5C**), which supports the physiological significance of GpsB-TarG interaction given that GpsB also localizes to nascent division sites (**Fig. 5B**; [15]). Division site localization of the WTA biosynthesis protein TarO (TagO) has also been noted in *S. aureus* [23]. The division site localization of TarO and TarG and their direct interaction between GpsB reveal that WTA machinery may be part of the divisome complex in *S. aureus*.

GpsB regulation of FtsZ is independent of wall teichoic acid synthesis

Our previous report showed that GpsB interacts with FtsZ and localizes to the site of division in *S. aureus*, so we wanted to see if GpsB localization at mid-cell was dependent on ongoing wall teichoic acid synthesis/export (**Fig. 5B**). For this purpose,

we used two inhibitors of wall teichoic acid synthesis, tunicamycin (early WTA biosynthesis by TarO is inhibited [24]) and targocil (TarGH-mediated WTA export is inhibited [25]). It is noteworthy that in addition to targeting TarO, tunicamycin could also target the early-stage peptidoglycan biosynthesis protein MraY at higher concentration [24]. Based on previous observations, treatment with these antibiotics does not halt cell division, however, the placement of the septa and overall regulation of division is disrupted. Treated cells also had significant cell separation defects presumably due to limited autolysin activity [24-28]. Given this information, we used high resolution fluorescence microscopy to monitor the localization of $GpsB^{SA}$-GFP in cells treated with tunicamycin or targocil. *S. aureus* cells containing $GpsB^{SA}$-GFP were grown to mid-log and then the inducer (IPTG) and the antibiotics (tunicamycin or targocil) were added, and cells were grown for an additional hour. At this point the majority of cells were expected to have completed a full round of division in our experimental condition. In the cultures treated with either tunicamycin or targocil, cells were significantly larger (**Figs. 5B and 5D**). The impaired autolytic activity is also evident with (25%) of cells having a completed septum designated “Stage 3” in the no antibiotic treatment control, vs (66%) in the tunicamycin treated cells and (78%) in the targocil treated cells (**Fig. 5C**). Despite the impaired cell separation in both the tunicamycin and targocil treated cells, we noted evidence of GpsB localizing to sites perpendicular to the previous plane of division (**Fig. 5B vi and ix**; white arrow heads) suggesting that although the cells are not separating properly, they are still attempting to undergo another round of division and that GpsB and presumably FtsZ localization/regulation remain intact. Interestingly, we did note one distinct phenotype between the tunicamycin and targocil treated cells. In the cells

367 treated with tunicamycin, GpsB-GFP appears to remain localized in the peripheral
368 membrane in addition to sites of division, however in the targocil treated cells there is
369 very little peripheral membrane localization (**Figs. 5B** panels **v and viii; and Fig. 5E**).
370
371 **Intragenic mutants reveal critical residues for GpsB/TarG interaction**
372 The homology modeling of our intragenic GpsB mutants revealed that three of the
373 mutations, ΔLEE, LEErpt, and R72H could disrupt protein-protein interactions. To
374 investigate whether any of these three mutations affected their localization, we imaged
375 these strains under fluorescence microscopy. As longer incubation with ΔLEE and
376 R72H is lethal (**Fig. S2C**), cells were imaged at an earlier time point (1 h post-
377 induction). We noted that all three mutations, ΔLEE, LEErpt, and R72H retained
378 wildtype-like localization (**Fig. 6A).** Next, we tested the ability of these mutants to
379 interact with TarG. Using the BACTH assay, we tested the interactions of ΔLEE,
380 LEErpt, and R72H with TarG. We observed that LEErpt and R72H were still able to
381 interact with TarG, however ΔLEE no longer interacted with TarG (**Fig. 6B**). This
382 suggests that the presence of these three residues (or the length of the disordered
383 linker connecting the N- and C-terminal domains) are important for the GpsB-TarG
384 interaction. As such, it is tempting to speculate whether the lethality of dominant ΔLEE
385 overproduction (**Fig. S2C**) could be due to the impairment of the native GpsB and TarG
386 interaction.
387
388 It has been reported that targocil treatment (inhibition of WTA export) could prevent the
389 translocation of major autolysin, Atl [28]. It was shown that *S. aureus* cells treated with

targocil exhibited reduced autolysis in comparison to untreated cells. We were interested in testing whether GpsB promoted or inhibited WTA export-mediated autolysis (**Fig. S5D**). The rate of autolysis did not change significantly between cells harboring an inducible copy of *gpsB*, *gpsB*$^{\Delta LEE}$, and the empty vector (EV) control. However, as reported previously, subsequent to targocil treatment, the strain harboring EV control displayed reduced autolysis. Interestingly, in targocil-treated cells overproducing GpsB, the autolysis was reproducibly higher compared to the EV control. This increased autolysis is dependent on TarG interaction, as overproduction of ΔLEE (which lacks the interaction with TarG; **Fig. 6B**) mimicked EV control. Thus, it appears that GpsB may facilitate autolysin (Atl) translocation through its interaction with the TarG component of the WTA export machinery.

DISCUSSION

GpsB is highly conserved across the Firmicute phylum. In *B. subtilis*, *S. pneumoniae*, and *L. monocytogenes*, GpsB is involved in the coordination of cell division and cell wall synthesis through the binding of PBPs and other partners [6, 7, 14]. Our lab recently reported a novel function of *S. aureus* GpsB in regulating FtsZ polymerization by promoting lateral interactions and facilitating GTP hydrolysis [15]. In this study, we characterized several different mutations in GpsB^{SA} in an effort to more thoroughly understand GpsB mediated cell division regulation in *S. aureus*. Subsequent to a suppressor screen, we identified TarG as a protein interaction partner of GpsB in *S. aureus* and found that residues 66-68 (LEE) of GpsB are critical for this interaction. An earlier BACTH investigation of *S. aureus* cell division factors and peptidoglycan

synthesis machinery identified an interaction between EzrA and GpsB, however it failed to show an interaction between GpsB and any other proteins including PBPs (PBP1, PBP2, and PBP3) [29]. However, it appears that GpsB may interact with PBP4 [22], which plays a role in peripheral peptidoglycan synthesis in *S. aureus* [30]. An extensive BACTH-based interaction analysis between lipoteichoic acid (LTA) biosynthesis proteins and cell division factors also revealed that GpsB is not part of the LTA complex in *S. aureus* [31]. Thus, our finding of TarG-GpsB interaction is insightful and was only suspected based on our unbiased approach. In addition to the GpsB interaction with TarG shown here, previous work showed that GpsB interacts with TarO in *S. aureus* (among other proteins) [22].

Traditionally, WTA export has been alluded to occur along the lateral cell wall with the possible help of shape-determining MreB, MreC, and/or MreD proteins in *B. subtilis* [21, 32-34], which could allow for higher order accumulation of WTA at lateral cell wall. Consistent with this model, several WTA biosynthesis proteins including TagGH also interacts with FtsEX which is involved in cell elongation in *B. subtilis* [35, 36]. However, evidence suggests that WTA synthesis is not only important for cell elongation as a role for FtsEX in cell division and cell separation has been elucidated in *S. pneumoniae* [37] (and it is also known that FtsEX can directly interact with FtsZ in the Gram-negative organism *E. coli* [38]). A role for FtsEX in the activation of a specific peptidoglycan hydrolase has been well documented in these organisms [36-39]. Additionally, of the proteins discussed above, MreC is a known interaction partner of GpsB in *B. subtilis*, *S. pneumoniae*, and *L. monocytogenes* [8, 14]. Interestingly, MreC and other GpsB

436 interaction partners, PBP1 and EzrA also interact with FtsEX in *B. subtilis* [35]. Thus, it
437 is possible to envision a complex made of Mre proteins, FtsEX, PBPs, and GpsB
438 moderating the WTA biosynthesis in *B. subtilis*. Although well-studied MreB is absent in
439 *S. aureus*, MreC and MreD proteins are present and are targeted to the division sites
440 [40], similar to GpsB [15]. Surprisingly, *S. aureus* lack the genes for FtsE and FtsX (L.
441 Aravind - National Center for Biotechnology Information/National Institutes of Health;
442 personal communication). During the course of evolution into a spherical organism from
443 a rod-shaped ancestor, it appears that *S. aureus* has lost the need for the FtsEX
444 complex. However, other alternate mechanism(s) to activate cell wall hydrolases, such
445 as LytH/ActH [41], exists. Thus, it is possible in *S. aureus* the WTA machinery is
446 positioned and regulated differently than its non-spherical counterparts in a manner that
447 involves GpsB.
448
449 There are several other lines of evidence that give additional credence to the GpsB-
450 WTA link. The first comes from the suppressor analysis in *L. monocytogenes* [42],
451 where Rismondo et al. show that suppressor mutations in the WTA biosynthesis
452 pathway can suppress the lethality of cells growing without *gpsB* at a higher non-
453 permissive temperature. These suppressors could be freeing lipid-II/UDP-GlcNAc for
454 the essential peptidoglycan biosynthesis pathway. It may be possible that several lipid-II
455 and/or UDP-GlcNAc utilizing WTA proteins and peptidoglycan synthesis components
456 could be streamlined with the help of GpsB as a central coordinator for efficient cell
457 cycle progression.
458

Another line of evidence supporting a GpsB-WTA link is the connection between WTA and division site localization/selection in multiple organisms. It has been shown that WTA machinery is enriched at the division site in both *B. subtilis* and *S. aureus* from the very start of septal membrane invagination [21, 23]. Interestingly, PBP4, a likely interaction partner of GpsB [22], depends on TarO for division site localization [23]. Investigations showed that inhibition of WTA synthesis [24, 43] or prevention of WTA transfer to peptidoglycan [44-46], affect the positioning of division septum in *S. aureus*, which indicate a direct or indirect role for WTA in division site selection. Of note, at least one of the WTA ligases in *S. aureus*, SA1195 (MsrR) may interact with GpsB [22]. Additionally, division site localization of lipoteichoic acids (LTA) synthesis complex in *S. aureus* has been noted previously [31] and it was shown that multiple proteins in the LTA machinery interact with the divisome, including PBPs and the well-characterized interaction partner of GpsB, EzrA. It is important to note that LTA synthesis happens extracellularly in the periplasmic space between the high-density cell wall zone and the membrane [47]. WTA synthesis on the other hand occurs intracellularly and is exported for covalent attachment to the peptidoglycan to be part of the high-density cell wall zone [47]. It is estimated that WTA makes up nearly 60% of the cell wall composition [19].

Evidence showing the presence of septal WTA is available [19, 24, 48, 49], and multiple studies have investigated the role and importance of WTA at sites of division. It has been proposed that the maturation (such as D-alanylation) and/or accumulation of WTA may then take place subsequent to cell division in order to not interfere with (or allow) the autolysin function [19, 23, 27, 50-53]. In support of this idea, it was reported that

LytF, a major autolysin in *B. subtilis*, is excluded from the lateral cell wall and localizes specifically to division sites in a WTA-dependent manner [33]. Perhaps autolysins interact with WTAs to allow for efficient separation of conjoined daughter cells in one, or a combination of, the following three ways: autolysins are actively recruited to the division sites with the aid of immature WTAs [51]; secretion of autolysins preferentially happen with WTA export at sites of division [28]; and/or septum-localized proteins such as FmtA selectively remove D-alanylation at the division site [54]. Additionally, other proteins that are translocated specifically at division sites, such as those with YSIRK signal, may rely on teichoic acids as well [55].

Taking the multiple lines of evidence into consideration, it is reasonable to postulate the presence of a multiprotein complex of complexes comprised of the divisome (including septal peptidoglycan synthesis components) and machineries involved in synthesizing both WTA and LTA at the site of cell division. As such, we propose a model taking previously published reports into account (**Fig. 7**). GpsB initially localizes to the sites of cell division in a FtsZ-dependent manner [15]. As shown in this study, TarG is preferentially enriched at the division site (**Fig. S5C**) and directly interacts with GpsB (**Fig. 5A**). Thus, we believe the TarGH WTA export complex and possibly TarO (based on its interaction with GpsB [22]; and enrichment at division site [23]) is recruited to the division site by GpsB in *S. aureus*. Subsequent to the creation of the highly crosslinked WTA-containing cell wall at the septum (shown as dark gray lines in **Fig. 7B and C**) and secretion of autolysin at the division site, regulated autolysis allows for daughter cell separation, within the scale of milliseconds [30, 56]. Immediately after cell separation,

peripherally-localized GpsB [15] may facilitate the continuous incorporation of WTA along the surface of the cell to further strengthen the cell envelope. Thus, we propose that GpsB aids in the coordination of cell division and WTA synthesis/export machineries in *S. aureus*. Further investigation is necessary to shed light on the dependency of multiple crucial cellular processes on GpsB and the nature of molecular interaction between GpsB and its multiple partners. Given the significance of GpsB in multiple cellular pathways, it is an attractive drug target for the development of anti-staphylococcal/antibiotic compounds.

MATERIALS AND METHODS

Suppressor Screen

Suppressor screening was carried out in the same manner as previously described [16]. Strain GG8 (*gpsB*^{SA}*-gfp*), was plated onto LB agar plates supplemented with 1 mM IPTG to induce expression of *gpsB*^{SA}*-gfp* and incubated at 37 °C overnight. Single colonies that were able to grow were then isolated from the plates and streaked onto new LB agar plates supplemented with 1 mM IPTG and incubated overnight at 37 °C. After confirming the ability of these strains to grow, genomic DNA was extracted and transformed into fresh wildtype PY79 cells and screened for *amyE* integration. These colonies were then streaked onto LB agar plates supplemented with 1 mM IPTG, with PY79 serving as the control, and incubated overnight at 37 °C. Strains that were not able to grow were denoted as possible extragenic mutations and sent for whole genome sequencing (MiGS Microbial Genome Sequencing center – Pittsburgh, PA). In contrast, any strains that were able to grow in the presence of the IPTG inducer were denoted as

528 possible **gpsB-gfp* intragenic suppressors. These strains were then screened via
529 fluorescence microscopy to detect GFP signal and rule out possible promoter or frame
530 shift mutations or the introduction of a premature stop codon. The genomic DNA from
531 the **gpsB-gfp* strains was isolated, the *amyE* locus carrying *gpsB-gfp* was PCR
532 amplified (op36/op24), and subsequently sequenced. Analysis of the sequences was
533 done using the ApE – A plasmid Editor (M. Wayne Davis), and multiple sequence
534 alignments were analyzed by using the Clustal Omega multiple sequence alignment
535 software [57].
536
537 **Strain construction**
538 All relevant strain and oligonucleotide information is listed in Table S1. Construction of
539 plasmids were performed with *E. coli* DH5α according to standard laboratory
540 procedures. To generate *B. subtilis* strains carrying both mutated (labelled collectively
541 as **gpsB-gfp)* and unmutated copies of *gpsB-gfp* we utilized a PY79 [58] derivative that
542 contains a second *amyE* locus (bkdB::Tn917::amyE::cat; Amy Camp). pGG4 [15] was
543 used to clone *gpsB-gfp* into the second *amyE* locus making strain LH72. The resistance
544 cassette was then switched from specR to ermR using pQP1 (Qi Pan) resulting in strain
545 LH73. Following screening, genomic DNA from the **gpsB-gfp* strains was transformed
546 into LH73 and colonies were screened for integration at the primary *amyE* locus. This
547 process resulted in strains LH75-LH80 that have IPTG inducible copies of both *gpsB-*
548 *gfp* and **gpsB-gfp*. Initial generation of *B. subtilis* strains containing the **gpsB-gfp*
549 mutations is described above (*See Suppressor Screen*). *S. aureus* strains were
550 constructed to place **gpsB-gfp* under the control of an IPTG inducible promoter using

the pCL15 plasmid backbone [59]. The plasmid containing unmutated GpsB-GFP, pPE46 [15] was transformed into RN4220 cells resulting in strain GGS2. DNA for Y14F, D41G, D41G, ΔLEE and R72H was PCR amplified (op36/oGG2; HindIII/SalI) and cloned into the pCL15 plasmid creating plasmids pLH5-pLH9. L35S and LEErpt were made though QuikChange (Agilent) of pPE46 resulting in pPE78 and pPE80. These plasmids were then transformed into RN4220 cells creating strains LH17-20, and LH35-LH36. These plasmids were also transformed into the *S. aureus* RN4220 Δ*spa* background (SEJ1; [60]) resulting in strains LH141-LH159. The untagged ΔLEE strain was similarly created through PCR amplification (op36/op38 HindIII/SphI) and cloned into the pCL15 plasmid background creating pAH1 and transformed into RN4220 cells resulting in strain AH2. Plasmids for Bacterial Two Hybrid analysis were created using pEB354 and pEB355 which carry the pUT25 and pUT18 subunits of adenylate cyclase respectively [17]. DNA for $GpsB^{SA}$ and $*GpsB^{SA}$ (BTH 11/BTH 12; EcoRI/XhoI) (LH39-LH40, LH43-56), TarG (BTH62/BTH63; EcoRI/Xho1) (SKB1-SKB2), and TarH (BTH 60/BTH61; EcoRI/Xho1) (SKB3-SKB4), was PCR amplified and cloned into both pEB354 and pEB355. To create the gfp-tagH strain in *B. subtilis* cells, chromosomal DNA from Bacillus Genetic Stock Center (BGSC) 1A1119 [21] was transformed into PY79 cells to create PE528. Similarly, to create the CRISPRi TagG/TagH strains, chromosomal DNA was extracted from strains BEC35710 and BEC35700 (from BGSC) respectively and transformed into PY79 cells to make SK15-SK16. Then, to create cells that contained the CRISPRi knockdown for TagG or TagH as well as IPTG inducible *$gpsB^{SA}$-gfp*, the same DNA was transformed into LH72 resulting in SK17-SK18. Finally, to create *gfp-tarG*, DNA was PCR amplified (oLH11/12; SalI/BamHI and oLH13/14;

574 BamHI/EcoRI) and ligated into the pJB67 vector [61] resulting in pLH64 which was then
575 transformed into RN4220 cells to make LH136.
576
577 **Spot Titer Assay**
578 The spot titer assays for *B. subtilis* strains were carried out on LB agar plates
579 supplemented with 1 mM IPTG where needed to induce the expression of *gpsB*^{SA}*-gfp* or
580 **gpsB*^{SA}*-gfp*. Cultures of the strains were first grown to mid-logarithmic phase
581 (OD_{600}=0.4-0.6) and subsequently standardized to OD_{600}=0.1. The standardized
582 cultures were then serially diluted and 1 µl of the liquid culture was spotted onto the
583 appropriate plate. These plates were then incubated overnight at 37 °C. Spot titer
584 assays for *S. aureus* strains were completed in the same manner using Tryptic Soy
585 Agar plates supplemented with 10 µg/ml chloramphenicol, and where needed, 1 mM
586 IPTG. The serial dilutions of the standardized cultures were spotted onto the plates with
587 a volume of 1 µl.
588
589 **Fluorescence Microscopy**
590 Florescence microscopy was carried out as previously described [62]. Overnight
591 cultures of *B. subtilis* strains in LB liquid media, or *S. aureus* strains in TSB
592 supplemented with 10 µg/ml chloramphenicol (pCL15 backbone) or 5 µg/ml
593 erythromycin (pJB67 backbone), were diluted to OD_{600}=0.1 and grown at 37 °C to mid
594 logarithmic phase (OD_{600}= 0.4-0.6). Then, for *B. subtilis* cultures, where needed, 1 mM
595 IPTG or 1% xylose was added to the cultures and grown for an additional 3 h. For *S.*
596 *aureus*, 1 mM IPTG (pCL15) or 1.25 µM $CdCl_2$ (pJB67) was added to the cultures

(except GFP-TarG where no inducer was added) and where needed, 20 µg/ml tunicamycin, or 8 µg/mL targocil was also added. Cells were then grown for an additional 1 h. Following incubation, 1 ml aliquots were then pelleted and resuspended in 100 µl PBS and 1 µg/ml SynaptoRed fluorescent dye to allow for visualization of the cell membranes. A culture aliquot (5 µl) was then transferred to a glass bottom dish (Mattek) and covered with a 1% agarose pad. Samples were imaged on a DeltaVision Core microscope system (Applied Precision/GE Healthcare) equipped with a Photometrics CoolSnap HQ2 camera and an environmental chamber. Seventeen planes were acquired every 200 nm and the data were deconvolved using SoftWorx software. Cell diameter was measured using ImageJ and analysis completed in GraphPad Prism 9.

Bacterial Two Hybrid Assay

Plasmids carrying our genes of interest were transformed into *E. coli* BTH101 cells and plated onto LB agar containing 100 µg/ml ampicillin and 50 µg/ml kanamycin and incubated at 30 °C for 48 h. A positive control strain was made by transforming PE87 and PE88 carrying pUT25-zip and pUT18-zip into the BTH101 cells. A negative control was made by transforming empty pEB354 and pEB355 into the cells. The resulting colonies harboring the pairs of plasmids of interest were then isolated and grown overnight in liquid LB media at 30 °C supplemented with 100 µg/ml ampicillin, 50 µg/ml kanamycin, and 0.5 mM IPTG. The following day, 2 µl of culture was spotted onto MacConkey plates (BD Biosciences) supplemented with 10 mg/ml maltose, 100 µg/ml ampicillin, 50 µg/ml kanamycin, and 0.5 mM IPTG. Plates were then incubated for 24 h

620 at 30 °C. β-galactosidase assays were completed in the 96 well plate reader as
621 previously described with some modification [63]. A mixture of 450 µl Z buffer, 120 µl
622 ONPG (4 mg/ml in Z buffer), 5.7 µl β-mercaptoethanol, 285 µl (polymyxin B 20 mg/ml),
623 and 60 µl of culture for each strain tested was prepared. 200 µl of each mixture was
624 then transferred in triplicate to a 96 well plate. Readings were taken in a BioTek plate
625 reader and Miller units calculated. Results were graphed using GraphPad Prism 9.
626

627 **Immunoblotting**

628 Cells were grown overnight and the next morning diluted to an OD_{600}=0.1. At OD_{600}=
629 0.4-0.6, IPTG was added to the appropriate cultures and then grown for an additional 1
630 h (*S. aureus*) or 3 h (*B. subtilis*). Aliquots of cultures (1 ml) were then collected and
631 pelleted. Cell lysis of *B. subtilis* cells was completed by using a protoplast buffer
632 containing 0.5 M sucrose, 20 mM $MgCl_2$, 10 mM KH_2PO_4, and 0.1 mg/ml lysozyme. *S.*
633 *aureus* cells (in RN4220 *Δspa* background [60]) were resuspended in 500 µl PBS with 5
634 µl lysostaphin (1 mg/ml in 20 mM sodium acetate) and incubated for 30 min at 37 °C. 1
635 µl of DNAse A (1U/µl) was then added and allowed to incubate for an additional 30 min.
636 Samples were then prepared for SDS-PAGE analysis. After electrophoresis, the
637 samples were transferred to a membrane and probed with rabbit antisera raised against
638 GFP (K. Ramamurthi) and SigA (M. Fujita) for *B. subtilis*, and GpsB-GFP for *S. aureus*
639 with total protein visualized using the GelCode Blue Safe Protein Stain (ThermoFisher).
640

641 **WTA Extraction**

WTAs were extracted and visualized as previously described [64]. Briefly, cultures of PES5 and PES13 were grown overnight and back diluted to an OD_{600} of 0.1 the next day. Cultures were then grown to mid-log before 1 mM IPTG was added, and then the cultures were grown for an additional 3 h. Cells were standardized to the same OD (OD_{600} of 1) and then pelleted and washed in SDS buffer. Cells were then boiled for 1 h and subsequently extensively washed in SDS buffer. The cells were then subjected to proteinase K treatment, and following washes in sterile distilled water, the WTAs were extracted with NaOH overnight. The following day the tubes were centrifuged to separate the WTA from leftover debris. The supernatant was then run on a Native PAGE gel and visualized with Alcian Blue (1:20 dilution of 1.25% stock solution in 2% acetic acid) followed by Silver Staining (ThermoFisher) following manufacturer protocols and imaged on the Bio-Rad Chemidoc MP Imaging System.

Autolysis Assay

Autolysis assays were carried out as previously described [28]. Overnight cultures were back diluted to an OD_{600} of 0.1. Cultures were grown at 37°C to mid-log (OD_{600} 0.4-0.6) and then 1mM IPTG was added and when needed targocil (5 µg/ml). Cells were then grown for an additional hour. Cells were then pelleted, washed twice in cold H_2O, and standardized to an OD_{600} of 0.8. Cells were then spun and resuspended in 0.5M Tris-HCl (pH 7.2) and 0.05% Triton -X 100. OD_{600} was monitored in a 96-well plate reader for 10 hours at 37°C. Results were graphed using Graphpad Prism 9.

Structural analysis and Multiple Sequence Alignment

664 The 3-dimensional model for the N-terminal domain of GpsB^{Sa} (res. 1-70) was
665 generated with the SWISS-MODEL homology-model server [18]. GpsB suppressor
666 mutants, and simulated interactions with homologous PBP complexes were generated
667 with PyMOL (Schrödinger, LLC). PDB coordinates for *S. pneumoniae*, *B. subtilis*, and *L.*
668 *monocytogenes* GpsB in complex with their associated PBPs were retrieved from the
669 PDB, with accession IDs 6GQN, 6GP7, and 6GPZ [14].
670

671 **ACKNOWLEDGEMENTS**
672
673 We thank our lab members for comments on the manuscript. This work was funded by
674 the National Institutes of Health grants (R35GM133617; PE) and (R21AI164775; YC
675 and PE).
676

677 **AUTHOR CONTRIBUTIONS**
678 The conception and design of the study (LH, CS, PE), data acquisition (LH, SK, MS,
679 AH, CS), analysis and/or interpretation of the data (LH, SK, MS, CS, YC, PE), and
680 writing of the manuscript (LH, MS, YC, PE).
681
682

683 **FIGURE LEGENDS**
684

685 **Figure 1**
686 GpsB^{SA}-GFP Suppressor Screen. (A) Cartoon diagram depicting workflow for GpsB^{SA}-
687 GFP suppressor screen. Figure generated using Biorender.com (B) Table describing

seven isolated GpsB^{SA}-GFP intragenic suppressor mutations detailing the mutation, amino acid change, and amino acid position. (C) Multiple sequence alignment of GpsB from *S. aureus*, *S. pneumoniae*, *B. subtilis*, and *L. monocytogenes*. Intragenic suppressor mutations identified in the GpsB^{SA}-GFP suppressor screen are highlighted in yellow and labeled above the residue locations. *, :, and ., indicate fully, strongly, or weakly conserved residues respectively. The structured N- and C-terminal domains are shown under the sequence alignment as reported previously [6].

Figure 2

Growth characteristics of intragenic suppressor mutations of GpsB^{SA}-GFP. (A) Spot titer assay of unmutated GpsB^{SA}-GFP (GG8) (top row) and isolated *GpsB^{SA}-GFP intragenic suppressor mutations (CS89-CS93, PE377, and PE448) were serially diluted, spotted on plates, and grown in the absence (left panel) or presence (right panel) of 1 mM IPTG. (B) Cell morphology of cells harboring unmutated GpsB^{SA}-GFP (GG8) and the *GpsB^{SA}-GFP intragenic suppressor mutations (CS89-CS93, PE377, and PE448) grown in the absence (i-viii) or presence (ix-xvi) of 1 mM IPTG. Images were taken 3 h after addition of inducer. Membrane was stained with SynaptoRed membrane dye. Scale bar is 1 µm.

Figure 3

Homology model of S. *aureus* GpsB. Residues mutated in the experiments are colored in yellow. The 8 residues of α-helix 2 S9-E15 are colored in blue. (A)The N-terminal domains of *S. pneumonia* PBP2a (PDB ID 6GQN, orange), *B. subtilis* PBP1a (PDB ID

6GP7, lavender) and *L. monocytogenes* PBPA1 (PDB ID 6GPZ, magenta) bound to GpsB were superimposed and are shown to illustrate the highly conserved PBP-binding groove. (B) The Y14F mutation occurs on α-helix 1 and points directly towards the putative PBP-binding partner. (C) The L35S mutation occurs at the junction of the hydrophobic, coiled-coiled core of α-helices $2_{A,B}$ and the PBP-binding groove. (D) The D41N, D41G mutations occur at the interface of the loop formed by the first 8 residues and the two adjacent helices of α-helix 2 from protomers A and B. (E) The LEELR sequence is the last of α helix 2 before it transitions into a disordered linker sequence that bridges the N-terminal domain to the C-terminal domain.

Figure 4

Analysis of $GpsB^{SA}$-GFP extragenic suppressor mutations. (A) Table describing the three isolated extragenic suppressor mutations detailing the specified gene, mutation, and amino acid change. (B) Fluorescence microscopy showing the cell morphology of strains containing a CRISPRi knockdown of *tagH* (SK16) and *tagG* (SK15) in *B. subtilis* grown in the absence (i and iii) and presence (ii and iv) of 1% xylose. (C) Cells containing inducible *gpsB*^{SA}*-gfp* (GG8) grown in the absence (i) and presence (ii) of 1 mM IPTG. Strains constructed to have both the CRISPRi knockdown of either *tagH* or *tagG* as well as inducible *gpsB*^{SA}*-gfp* (SK18 and SK17) were imaged in the absence of xylose and IPTG (iii and vii), in the presence of xylose only (v and ix), in the presence IPTG only (iv and viii), and finally in the presence of both xylose and IPTG (vi and x). Cells imaged 3 h after the addition of xylose and/or IPTG. Scale bar 1 µm. (D) Fluorescence micrographs tracking the localization pattern of $GpsB^{BS}$-GFP (i – iii) and

734 GFP-TagH^{BS} (PE528) (iv – vi) through different stages of the cell division (see
735 arrowheads). Cell membrane is visualized with SynaptoRed membrane dye. Scale bar 1
736 µm.
737
738 **Figure 5**
739 Characterization of the link between WTA exporter TarGH and GpsB in *S. aureus*. (A)
740 Bacterial Two Hybrid Assay to investigate pairwise interactions of GpsB^{SA} with *S.*
741 *aureus* TarG (SKB1 and SKB2) and TarH (SKB3 and SKB4). A color change to deep
742 pink indicates a positive interaction. Images taken after 24 h of incubation. (B)
743 Localization pattern of GpsB^{SA}-GFP (PES6) in SH1000 *S. aureus* cells following 1 h of
744 treatment with 20 µg/ml tunicamycin (iv-vi) or 8 µg/mL targocil (vii-ix). White arrowheads
745 show instances of GpsB^{SA}-GFP localizing to the next division site despite incomplete
746 cell separation. Cell membranes visualized with SynaptoRed membrane dye. Scale bar
747 is 1 µm. (C) Number of cells in each stage of division following 1 h of treatment with
748 tunicamycin or targocil. Stage 1 (black bars) cells show no membrane enrichment at
749 mid-cell. Stage 2 cells (pink bars) have some membrane enrichment at mid-cell but do
750 not have fully formed septa. Stage 3 (teal bars) are cells that have fully formed septa at
751 mid-cell. (D) Quantification of cell diameters from Stage 3 cells treated with tunicamycin
752 or targocil, n = 100 cells, *** P = 0.0002, **** P < 0.0001. One-way ANOVA analysis and
753 multiple comparisons performed in GraphPad Prism 9. (E) Number of Stage 3 cells
754 showing localization of GpsB-GFP at the division site only (grey) or at the division site
755 and the periphery (purple) following 1 h of treatment of tunicamycin or targocil n = 100
756 cells.

Figure 6

Characterizing GpsB residues important for TarG interaction. (A) Localization pattern of GpsB-GFP (GGS2) or *GpsB-GFP (ΔLEE, LEErpt, R72H) (LH17, LH35, LH18) in RN4220 *S. aureus* cells. Cells imaged 1 h after the addition of 1 mM IPTG and stained with SynaptoRed membrane dye. Scale bar is 1 μm. (B) Bacterial Two Hybrid Assay of pairwise interactions of TarG (SKB2) and GpsB (LH39) or *GpsB (ΔLEE, LEErpt, R72H) (LH47, LH43, LH55). A color change to deep pink indicates a positive interaction. Images taken after 24 h of incubation.

Figure 7

Model of GpsB-mediated coordination of cell division and wall teichoic acid export. (A) GpsB localizes to the division site in a FtsZ dependent manner [15]. (B) At the onset of membrane invagination, GpsB recruits WTA export machinery to the site of cell division. (C) Autolysins specifically act at the division septum to detach the daughter cells. GpsB – green; TarGH – blue; Autolysins – red; membrane – orange; light & dark gray – less-crosslinked cell wall and WTA-rich highly-crosslinked cell wall respectively [24, 48, 49].

REFERENCES

1. Haeusser DP, Margolin W. Splitsville: structural and functional insights into the dynamic bacterial Z ring. Nat Rev Microbiol. 2016;14(5):305-19. Epub 2016/04/05. doi: 10.1038/nrmicro.2016.26. PubMed PMID: 27040757; PubMed Central PMCID: PMCPMC5290750.
2. Eswara PJ, Ramamurthi KS. Bacterial Cell Division: Nonmodels Poised to Take the Spotlight. Annu Rev Microbiol. 2017;71:393-411. Epub 2017/07/13. doi:

783 10.1146/annurev-micro-102215-095657. PubMed PMID: 28697666; PubMed Central
784 PMCID: PMCPMC6291244.
785 3. Errington J, Wu LJ. Cell Cycle Machinery in Bacillus subtilis. Subcell Biochem.
786 2017;84:67-101. Epub 2017/05/14. doi: 10.1007/978-3-319-53047-5_3. PubMed PMID:
787 28500523; PubMed Central PMCID: PMCPMC6126333.
788 4. Egan AJF, Errington J, Vollmer W. Regulation of peptidoglycan synthesis and
789 remodelling. Nat Rev Microbiol. 2020;18(8):446-60. Epub 2020/05/20. doi:
790 10.1038/s41579-020-0366-3. PubMed PMID: 32424210.
791 5. Pinho MG, Kjos M, Veening JW. How to get (a)round: mechanisms controlling
792 growth and division of coccoid bacteria. Nat Rev Microbiol. 2013;11(9):601-14. Epub
793 2013/08/21. doi: 10.1038/nrmicro3088. PubMed PMID: 23949602.
794 6. Halbedel S, Lewis RJ. Structural basis for interaction of DivIVA/GpsB proteins
795 with their ligands. Mol Microbiol. 2019;111(6):1404-15. Epub 2019/03/20. doi:
796 10.1111/mmi.14244. PubMed PMID: 30887576.
797 7. Hammond LR, White ML, Eswara PJ. ¡vIVA la DivIVA! J Bacteriol. 2019;201(21).
798 Epub 2019/08/14. doi: 10.1128/JB.00245-19. PubMed PMID: 31405912; PubMed
799 Central PMCID: PMCPMC6779457.
800 8. Claessen D, Emmins R, Hamoen LW, Daniel RA, Errington J, Edwards DH.
801 Control of the cell elongation-division cycle by shuttling of PBP1 protein in Bacillus
802 subtilis. Mol Microbiol. 2008;68(4):1029-46. Epub 2008/03/28. doi: 10.1111/j.1365-
803 2958.2008.06210.x. PubMed PMID: 18363795.
804 9. Tavares JR, de Souza RF, Meira GL, Gueiros-Filho FJ. Cytological
805 characterization of YpsB, a novel component of the Bacillus subtilis divisome. J
806 Bacteriol. 2008;190(21):7096-107. Epub 2008/09/09. doi: 10.1128/JB.00064-08.
807 PubMed PMID: 18776011; PubMed Central PMCID: PMCPMC2580690.
808 10. Rismondo J, Cleverley RM, Lane HV, Grosshennig S, Steglich A, Moller L, et al.
809 Structure of the bacterial cell division determinant GpsB and its interaction with
810 penicillin-binding proteins. Mol Microbiol. 2016;99(5):978-98. Epub 2015/11/18. doi:
811 10.1111/mmi.13279. PubMed PMID: 26575090.
812 11. Land AD, Tsui HC, Kocaoglu O, Vella SA, Shaw SL, Keen SK, et al.
813 Requirement of essential Pbp2x and GpsB for septal ring closure in Streptococcus
814 pneumoniae D39. Mol Microbiol. 2013;90(5):939-55. Epub 2013/10/15. doi:
815 10.1111/mmi.12408. PubMed PMID: 24118410; PubMed Central PMCID:
816 PMCPMC4120849.
817 12. Fleurie A, Manuse S, Zhao C, Campo N, Cluzel C, Lavergne JP, et al. Interplay
818 of the serine/threonine-kinase StkP and the paralogs DivIVA and GpsB in
819 pneumococcal cell elongation and division. PLoS Genet. 2014;10(4):e1004275. Epub
820 2014/04/12. doi: 10.1371/journal.pgen.1004275. PubMed PMID: 24722178; PubMed
821 Central PMCID: PMCPMC3983041.
822 13. Rued BE, Zheng JJ, Mura A, Tsui HT, Boersma MJ, Mazny JL, et al.
823 Suppression and synthetic-lethal genetic relationships of DeltagpsB mutations indicate
824 that GpsB mediates protein phosphorylation and penicillin-binding protein interactions in
825 Streptococcus pneumoniae D39. Mol Microbiol. 2017;103(6):931-57. Epub 2016/12/24.
826 doi: 10.1111/mmi.13613. PubMed PMID: 28010038; PubMed Central PMCID:
827 PMCPMC5344783.

14. Cleverley RM, Rutter ZJ, Rismondo J, Corona F, Tsui HT, Alatawi FA, et al. The cell cycle regulator GpsB functions as cytosolic adaptor for multiple cell wall enzymes. Nat Commun. 2019;10(1):261. Epub 2019/01/18. doi: 10.1038/s41467-018-08056-2. PubMed PMID: 30651563; PubMed Central PMCID: PMCPMC6335420.
15. Eswara PJ, Brzozowski RS, Viola MG, Graham G, Spanoudis C, Trebino C, et al. An essential Staphylococcus aureus cell division protein directly regulates FtsZ dynamics. Elife. 2018;7. Epub 2018/10/03. doi: 10.7554/eLife.38856. PubMed PMID: 30277210; PubMed Central PMCID: PMCPMC6168285.
16. Brzozowski RS, Tomlinson BR, Sacco MD, Chen JJ, Ali AN, Chen Y, et al. Interdependent YpsA- and YfhS-Mediated Cell Division and Cell Size Phenotypes in Bacillus subtilis. mSphere. 2020;5(4). Epub 2020/07/24. doi: 10.1128/mSphere.00655-20. PubMed PMID: 32699122; PubMed Central PMCID: PMCPMC7376506.
17. Battesti A, Bouveret E. The bacterial two-hybrid system based on adenylate cyclase reconstitution in Escherichia coli. Methods. 2012;58(4):325-34. Epub 2012/07/31. doi: 10.1016/j.ymeth.2012.07.018. PubMed PMID: 22841567.
18. Schwede T, Kopp J, Guex N, Peitsch MC. SWISS-MODEL: An automated protein homology-modeling server. Nucleic Acids Res. 2003;31(13):3381-5. Epub 2003/06/26. doi: 10.1093/nar/gkg520. PubMed PMID: 12824332; PubMed Central PMCID: PMCPMC168927.
19. Brown S, Santa Maria JP, Jr., Walker S. Wall teichoic acids of gram-positive bacteria. Annu Rev Microbiol. 2013;67:313-36. Epub 2013/09/13. doi: 10.1146/annurev-micro-092412-155620. PubMed PMID: 24024634; PubMed Central PMCID: PMCPMC3883102.
20. Peters JM, Colavin A, Shi H, Czarny TL, Larson MH, Wong S, et al. A Comprehensive, CRISPR-based Functional Analysis of Essential Genes in Bacteria. Cell. 2016;165(6):1493-506. Epub 2016/05/31. doi: 10.1016/j.cell.2016.05.003. PubMed PMID: 27238023; PubMed Central PMCID: PMCPMC4894308.
21. Formstone A, Carballido-Lopez R, Noirot P, Errington J, Scheffers DJ. Localization and interactions of teichoic acid synthetic enzymes in Bacillus subtilis. J Bacteriol. 2008;190(5):1812-21. Epub 2007/12/25. doi: 10.1128/JB.01394-07. PubMed PMID: 18156271; PubMed Central PMCID: PMCPMC2258661.
22. Kent VL. Cell wall architecture and the role of wall teichoic acid in *Staphylococcus aureus*. White Rose eTheses Online: University of Sheffield; 2013.
23. Atilano ML, Pereira PM, Yates J, Reed P, Veiga H, Pinho MG, et al. Teichoic acids are temporal and spatial regulators of peptidoglycan cross-linking in Staphylococcus aureus. Proc Natl Acad Sci U S A. 2010;107(44):18991-6. Epub 2010/10/15. doi: 10.1073/pnas.1004304107. PubMed PMID: 20944066; PubMed Central PMCID: PMCPMC2973906.
24. Campbell J, Singh AK, Santa Maria JP, Jr., Kim Y, Brown S, Swoboda JG, et al. Synthetic lethal compound combinations reveal a fundamental connection between wall teichoic acid and peptidoglycan biosyntheses in Staphylococcus aureus. ACS Chem Biol. 2011;6(1):106-16. Epub 2010/10/22. doi: 10.1021/cb100269f. PubMed PMID: 20961110; PubMed Central PMCID: PMCPMC3025082.
25. Campbell J, Singh AK, Swoboda JG, Gilmore MS, Wilkinson BJ, Walker S. An antibiotic that inhibits a late step in wall teichoic acid biosynthesis induces the cell wall stress stimulon in Staphylococcus aureus. Antimicrob Agents Chemother.

2012;56(4):1810-20. Epub 2012/02/01. doi: 10.1128/AAC.05938-11. PubMed PMID: 22290958; PubMed Central PMCID: PMCPMC3318382.

26. Biswas R, Martinez RE, Gohring N, Schlag M, Josten M, Xia G, et al. Proton-binding capacity of Staphylococcus aureus wall teichoic acid and its role in controlling autolysin activity. PLoS One. 2012;7(7):e41415. Epub 2012/08/23. doi: 10.1371/journal.pone.0041415. PubMed PMID: 22911791; PubMed Central PMCID: PMCPMC3402425.

27. Schlag M, Biswas R, Krismer B, Kohler T, Zoll S, Yu W, et al. Role of staphylococcal wall teichoic acid in targeting the major autolysin Atl. Mol Microbiol. 2010;75(4):864-73. Epub 2010/01/29. doi: 10.1111/j.1365-2958.2009.07007.x. PubMed PMID: 20105277.

28. Tiwari KB, Gatto C, Walker S, Wilkinson BJ. Exposure of Staphylococcus aureus to Targocil Blocks Translocation of the Major Autolysin Atl across the Membrane, Resulting in a Significant Decrease in Autolysis. Antimicrob Agents Chemother. 2018;62(7). Epub 2018/05/08. doi: 10.1128/AAC.00323-18. PubMed PMID: 29735561; PubMed Central PMCID: PMCPMC6021642.

29. Steele VR, Bottomley AL, Garcia-Lara J, Kasturiarachchi J, Foster SJ. Multiple essential roles for EzrA in cell division of Staphylococcus aureus. Mol Microbiol. 2011;80(2):542-55. Epub 2011/03/16. doi: 10.1111/j.1365-2958.2011.07591.x. PubMed PMID: 21401734.

30. Monteiro JM, Fernandes PB, Vaz F, Pereira AR, Tavares AC, Ferreira MT, et al. Cell shape dynamics during the staphylococcal cell cycle. Nat Commun. 2015;6:8055. Epub 2015/08/19. doi: 10.1038/ncomms9055. PubMed PMID: 26278781; PubMed Central PMCID: PMCPMC4557339.

31. Reichmann NT, Picarra Cassona C, Monteiro JM, Bottomley AL, Corrigan RM, Foster SJ, et al. Differential localization of LTA synthesis proteins and their interaction with the cell division machinery in Staphylococcus aureus. Mol Microbiol. 2014;92(2):273-86. Epub 2014/02/19. doi: 10.1111/mmi.12551. PubMed PMID: 24533796; PubMed Central PMCID: PMCPMC4065355.

32. Schirner K, Marles-Wright J, Lewis RJ, Errington J. Distinct and essential morphogenic functions for wall- and lipo-teichoic acids in Bacillus subtilis. EMBO J. 2009;28(7):830-42. Epub 2009/02/21. doi: 10.1038/emboj.2009.25. PubMed PMID: 19229300; PubMed Central PMCID: PMCPMC2670855.

33. Yamamoto H, Miyake Y, Hisaoka M, Kurosawa S, Sekiguchi J. The major and minor wall teichoic acids prevent the sidewall localization of vegetative DL-endopeptidase LytF in Bacillus subtilis. Mol Microbiol. 2008;70(2):297-310. Epub 2008/09/03. doi: 10.1111/j.1365-2958.2008.06397.x. PubMed PMID: 18761696.

34. Kawai Y, Marles-Wright J, Cleverley RM, Emmins R, Ishikawa S, Kuwano M, et al. A widespread family of bacterial cell wall assembly proteins. EMBO J. 2011;30(24):4931-41. Epub 2011/10/04. doi: 10.1038/emboj.2011.358. PubMed PMID: 21964069; PubMed Central PMCID: PMCPMC3243631.

35. Dominguez-Cuevas P, Porcelli I, Daniel RA, Errington J. Differentiated roles for MreB-actin isologues and autolytic enzymes in Bacillus subtilis morphogenesis. Mol Microbiol. 2013;89(6):1084-98. Epub 2013/07/23. doi: 10.1111/mmi.12335. PubMed PMID: 23869552; PubMed Central PMCID: PMCPMC3817527.

36. Meisner J, Montero Llopis P, Sham LT, Garner E, Bernhardt TG, Rudner DZ. FtsEX is required for CwlO peptidoglycan hydrolase activity during cell wall elongation in Bacillus subtilis. Mol Microbiol. 2013;89(6):1069-83. Epub 2013/07/17. doi: 10.1111/mmi.12330. PubMed PMID: 23855774; PubMed Central PMCID: PMCPMC3786131.
37. Sham LT, Barendt SM, Kopecky KE, Winkler ME. Essential PcsB putative peptidoglycan hydrolase interacts with the essential FtsXSpn cell division protein in Streptococcus pneumoniae D39. Proc Natl Acad Sci U S A. 2011;108(45):E1061-9. Epub 2011/10/19. doi: 10.1073/pnas.1108323108. PubMed PMID: 22006325; PubMed Central PMCID: PMCPMC3215045.
38. Du S, Henke W, Pichoff S, Lutkenhaus J. How FtsEX localizes to the Z ring and interacts with FtsA to regulate cell division. Mol Microbiol. 2019;112(3):881-95. Epub 2019/06/09. doi: 10.1111/mmi.14324. PubMed PMID: 31175681; PubMed Central PMCID: PMCPMC6831102.
39. Pichoff S, Du S, Lutkenhaus J. Roles of FtsEX in cell division. Res Microbiol. 2019;170(8):374-80. Epub 2019/08/04. doi: 10.1016/j.resmic.2019.07.003. PubMed PMID: 31376483; PubMed Central PMCID: PMCPMC6899183.
40. Tavares AC, Fernandes PB, Carballido-Lopez R, Pinho MG. MreC and MreD Proteins Are Not Required for Growth of Staphylococcus aureus. PLoS One. 2015;10(10):e0140523. Epub 2015/10/16. doi: 10.1371/journal.pone.0140523. PubMed PMID: 26470021; PubMed Central PMCID: PMCPMC4607420.
41. Do T, Schaefer K, Santiago AG, Coe KA, Fernandes PB, Kahne D, et al. Staphylococcus aureus cell growth and division are regulated by an amidase that trims peptides from uncrosslinked peptidoglycan. Nat Microbiol. 2020;5(2):291-303. Epub 2020/01/15. doi: 10.1038/s41564-019-0632-1. PubMed PMID: 31932712; PubMed Central PMCID: PMCPMC7046134.
42. Rismondo J, Bender JK, Halbedel S. Suppressor Mutations Linking gpsB with the First Committed Step of Peptidoglycan Biosynthesis in Listeria monocytogenes. J Bacteriol. 2017;199(1). Epub 2016/11/01. doi: 10.1128/JB.00393-16. PubMed PMID: 27795316; PubMed Central PMCID: PMCPMC5165104.
43. Santa Maria JP, Jr., Sadaka A, Moussa SH, Brown S, Zhang YJ, Rubin EJ, et al. Compound-gene interaction mapping reveals distinct roles for Staphylococcus aureus teichoic acids. Proc Natl Acad Sci U S A. 2014;111(34):12510-5. Epub 2014/08/12. doi: 10.1073/pnas.1404099111. PubMed PMID: 25104751; PubMed Central PMCID: PMCPMC4151746.
44. Over B, Heusser R, McCallum N, Schulthess B, Kupferschmied P, Gaiani JM, et al. LytR-CpsA-Psr proteins in Staphylococcus aureus display partial functional redundancy and the deletion of all three severely impairs septum placement and cell separation. FEMS Microbiol Lett. 2011;320(2):142-51. Epub 2011/05/11. doi: 10.1111/j.1574-6968.2011.02303.x. PubMed PMID: 21554381.
45. Chan YG, Frankel MB, Dengler V, Schneewind O, Missiakas D. Staphylococcus aureus mutants lacking the LytR-CpsA-Psr family of enzymes release cell wall teichoic acids into the extracellular medium. J Bacteriol. 2013;195(20):4650-9. Epub 2013/08/13. doi: 10.1128/JB.00544-13. PubMed PMID: 23935043; PubMed Central PMCID: PMCPMC3807444.

964 46. Li FKK, Rosell FI, Gale RT, Simorre JP, Brown ED, Strynadka NCJ.
965 Crystallographic analysis of Staphylococcus aureus LcpA, the primary wall teichoic acid
966 ligase. J Biol Chem. 2020;295(9):2629-39. Epub 2020/01/24. doi:
967 10.1074/jbc.RA119.011469. PubMed PMID: 31969390; PubMed Central PMCID:
968 PMCPMC7049971.
969 47. Reichmann NT, Grundling A. Location, synthesis and function of glycolipids and
970 polyglycerolphosphate lipoteichoic acid in Gram-positive bacteria of the phylum
971 Firmicutes. FEMS Microbiol Lett. 2011;319(2):97-105. Epub 2011/03/11. doi:
972 10.1111/j.1574-6968.2011.02260.x. PubMed PMID: 21388439; PubMed Central
973 PMCID: PMCPMC3089915.
974 48. Matias VR, Beveridge TJ. Cryo-electron microscopy of cell division in
975 Staphylococcus aureus reveals a mid-zone between nascent cross walls. Mol Microbiol.
976 2007;64(1):195-206. Epub 2007/03/23. doi: 10.1111/j.1365-2958.2007.05634.x.
977 PubMed PMID: 17376082.
978 49. Matias VR, Beveridge TJ. Native cell wall organization shown by cryo-electron
979 microscopy confirms the existence of a periplasmic space in Staphylococcus aureus. J
980 Bacteriol. 2006;188(3):1011-21. Epub 2006/01/24. doi: 10.1128/JB.188.3.1011-
981 1021.2006. PubMed PMID: 16428405; PubMed Central PMCID: PMCPMC1347357.
982 50. Nega M, Tribelli PM, Hipp K, Stahl M, Gotz F. New insights in the coordinated
983 amidase and glucosaminidase activity of the major autolysin (Atl) in Staphylococcus
984 aureus. Commun Biol. 2020;3(1):695. Epub 2020/11/22. doi: 10.1038/s42003-020-
985 01405-2. PubMed PMID: 33219282; PubMed Central PMCID: PMCPMC7679415.
986 51. Bonnet J, Durmort C, Mortier-Barriere I, Campo N, Jacq M, Moriscot C, et al.
987 Nascent teichoic acids insertion into the cell wall directs the localization and activity of
988 the major pneumococcal autolysin LytA. Cell Surf. 2018;2:24-37. Epub 2018/06/12. doi:
989 10.1016/j.tcsw.2018.05.001. PubMed PMID: 32743129; PubMed Central PMCID:
990 PMCPMC7389264.
991 52. Frankel MB, Schneewind O. Determinants of murein hydrolase targeting to
992 cross-wall of Staphylococcus aureus peptidoglycan. J Biol Chem. 2012;287(13):10460-
993 71. Epub 2012/02/04. doi: 10.1074/jbc.M111.336404. PubMed PMID: 22303016;
994 PubMed Central PMCID: PMCPMC3323028.
995 53. Qamar A, Golemi-Kotra D. Dual roles of FmtA in Staphylococcus aureus cell wall
996 biosynthesis and autolysis. Antimicrob Agents Chemother. 2012;56(7):3797-805. Epub
997 2012/05/09. doi: 10.1128/AAC.00187-12. PubMed PMID: 22564846; PubMed Central
998 PMCID: PMCPMC3393393.
999 54. Rahman MM, Hunter HN, Prova S, Verma V, Qamar A, Golemi-Kotra D. The
1000 Staphylococcus aureus Methicillin Resistance Factor FmtA Is a d-Amino Esterase That
1001 Acts on Teichoic Acids. mBio. 2016;7(1):e02070-15. Epub 2016/02/11. doi:
1002 10.1128/mBio.02070-15. PubMed PMID: 26861022; PubMed Central PMCID:
1003 PMCPMC4752606.
1004 55. Zhang R, Shebes MA, Kho K, Scaffidi SJ, Meredith TC, Yu W. Spatial regulation
1005 of protein A in Staphylococcus aureus. Mol Microbiol. 2021. Epub 2021/05/06. doi:
1006 10.1111/mmi.14734. PubMed PMID: 33949015.
1007 56. Zhou X, Halladin DK, Rojas ER, Koslover EF, Lee TK, Huang KC, et al. Bacterial
1008 division. Mechanical crack propagation drives millisecond daughter cell separation in
1009 Staphylococcus aureus. Science. 2015;348(6234):574-8. Epub 2015/05/02. doi:

10.1126/science.aaa1511. PubMed PMID: 25931560; PubMed Central PMCID: PMCPMC4864021.

57. Sievers F, Wilm A, Dineen D, Gibson TJ, Karplus K, Li W, et al. Fast, scalable generation of high-quality protein multiple sequence alignments using Clustal Omega. Mol Syst Biol. 2011;7:539. Epub 2011/10/13. doi: 10.1038/msb.2011.75. PubMed PMID: 21988835; PubMed Central PMCID: PMCPMC3261699.

58. Youngman P, Perkins JB, Losick R. Construction of a cloning site near one end of Tn917 into which foreign DNA may be inserted without affecting transposition in Bacillus subtilis or expression of the transposon-borne erm gene. Plasmid. 1984;12(1):1-9. Epub 1984/07/01. doi: 10.1016/0147-619x(84)90061-1. PubMed PMID: 6093169.

59. Luong TT, Lee CY. The arl locus positively regulates Staphylococcus aureus type 5 capsule via an mgrA-dependent pathway. Microbiology (Reading). 2006;152(Pt 10):3123-31. Epub 2006/09/29. doi: 10.1099/mic.0.29177-0. PubMed PMID: 17005991.

60. Yu W, Missiakas D, Schneewind O. Septal secretion of protein A in Staphylococcus aureus requires SecA and lipoteichoic acid synthesis. Elife. 2018;7. Epub 2018/05/15. doi: 10.7554/eLife.34092. PubMed PMID: 29757141; PubMed Central PMCID: PMCPMC5962339.

61. Windham IH, Chaudhari SS, Bose JL, Thomas VC, Bayles KW. SrrAB Modulates Staphylococcus aureus Cell Death through Regulation of cidABC Transcription. J Bacteriol. 2016;198(7):1114-22. Epub 2016/01/27. doi: 10.1128/JB.00954-15. PubMed PMID: 26811317; PubMed Central PMCID: PMCPMC4800867.

62. Brzozowski RS, White ML, Eswara PJ. Live-Cell Fluorescence Microscopy to Investigate Subcellular Protein Localization and Cell Morphology Changes in Bacteria. J Vis Exp. 2019;(153). Epub 2019/12/10. doi: 10.3791/59905. PubMed PMID: 31814606; PubMed Central PMCID: PMCPMC7409980.

63. Priest DG, Cui L, Kumar S, Dunlap DD, Dodd IB, Shearwin KE. Quantitation of the DNA tethering effect in long-range DNA looping in vivo and in vitro using the Lac and lambda repressors. Proc Natl Acad Sci U S A. 2014;111(1):349-54. Epub 2013/12/18. doi: 10.1073/pnas.1317817111. PubMed PMID: 24344307; PubMed Central PMCID: PMCPMC3890862.

64. Kho K, Meredith TC. Salt-Induced Stress Stimulates a Lipoteichoic Acid-Specific Three-Component Glycosylation System in Staphylococcus aureus. J Bacteriol. 2018;200(12). Epub 2018/04/11. doi: 10.1128/JB.00017-18. PubMed PMID: 29632092; PubMed Central PMCID: PMCPMC5971477.

A

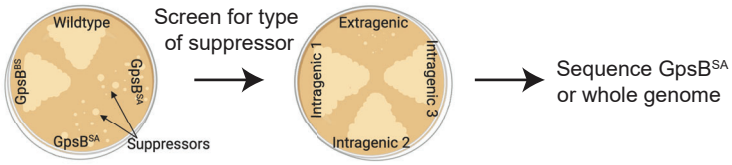

B

Suppressor #	*Mutation*	*Amino Acid Change*	*Position*
1	TAT to TTT	Y14F	14
2	TTA to TCA	L35S	35
3	GAT to GGT	D41G	41
4	GAT to AAT	D41N	41
5	(TTAGAAGAA) deletion	ΔLEE	66-68
6	(TTAGAAGAA) repeat	LEErpt	66-68
7	CGT to CAT	R72H	72

C

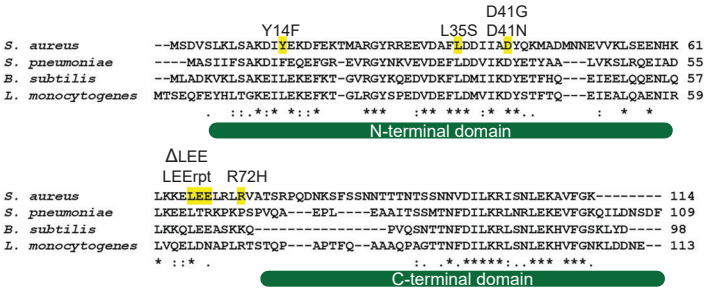

Figure 1

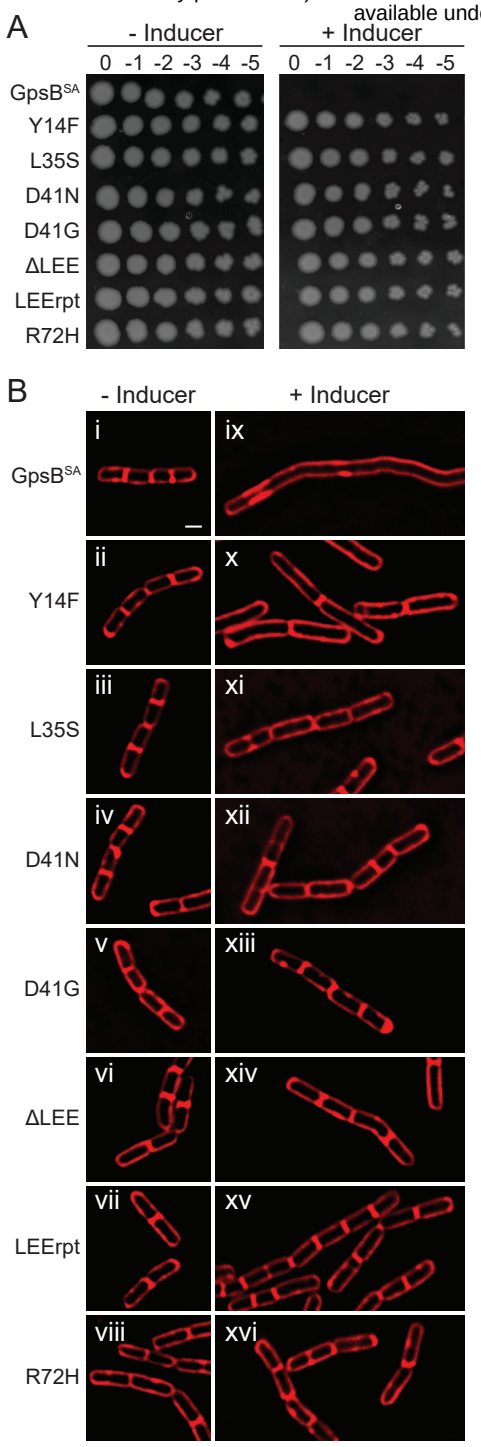

Figure 2

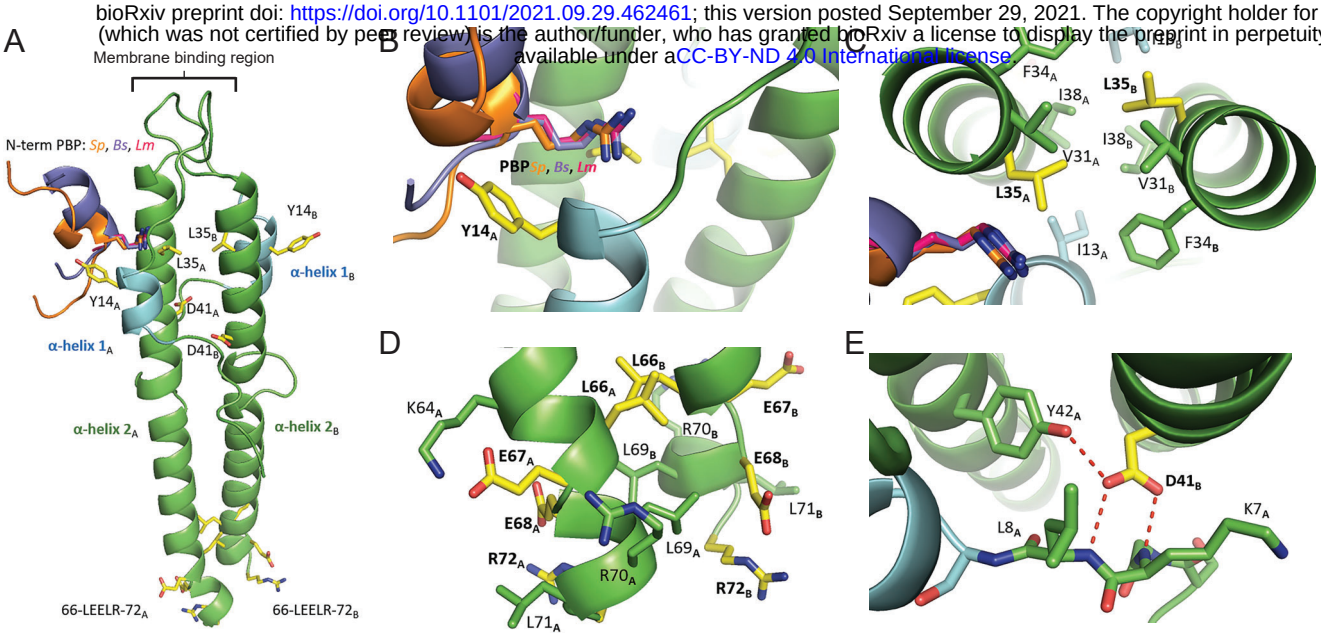

Figure 3

A

Suppressor #	*Gene*	*Mutation*	*Amino Acid Change*
1	*tagH*	TAC to TGC	Y233C
2	*tagH*	TAC to TGC	Y233C
3	*tagG*	AGA to AAA	R20K

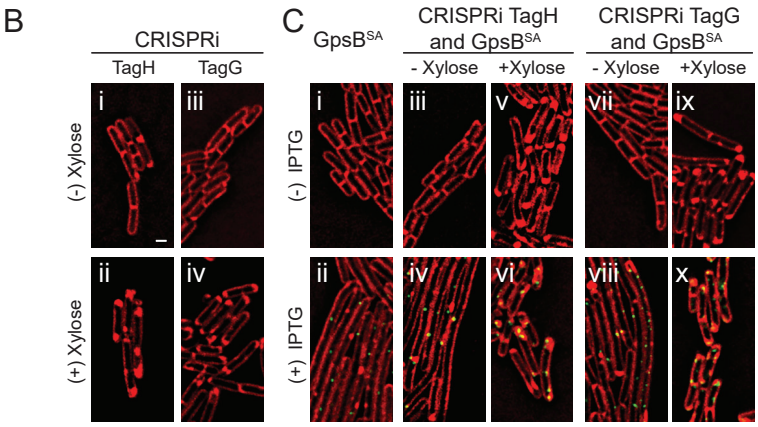

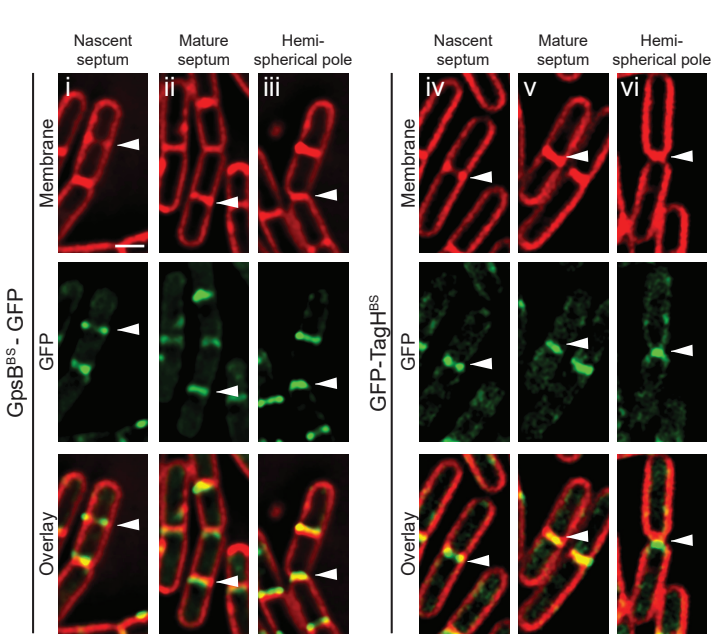

Figure 4

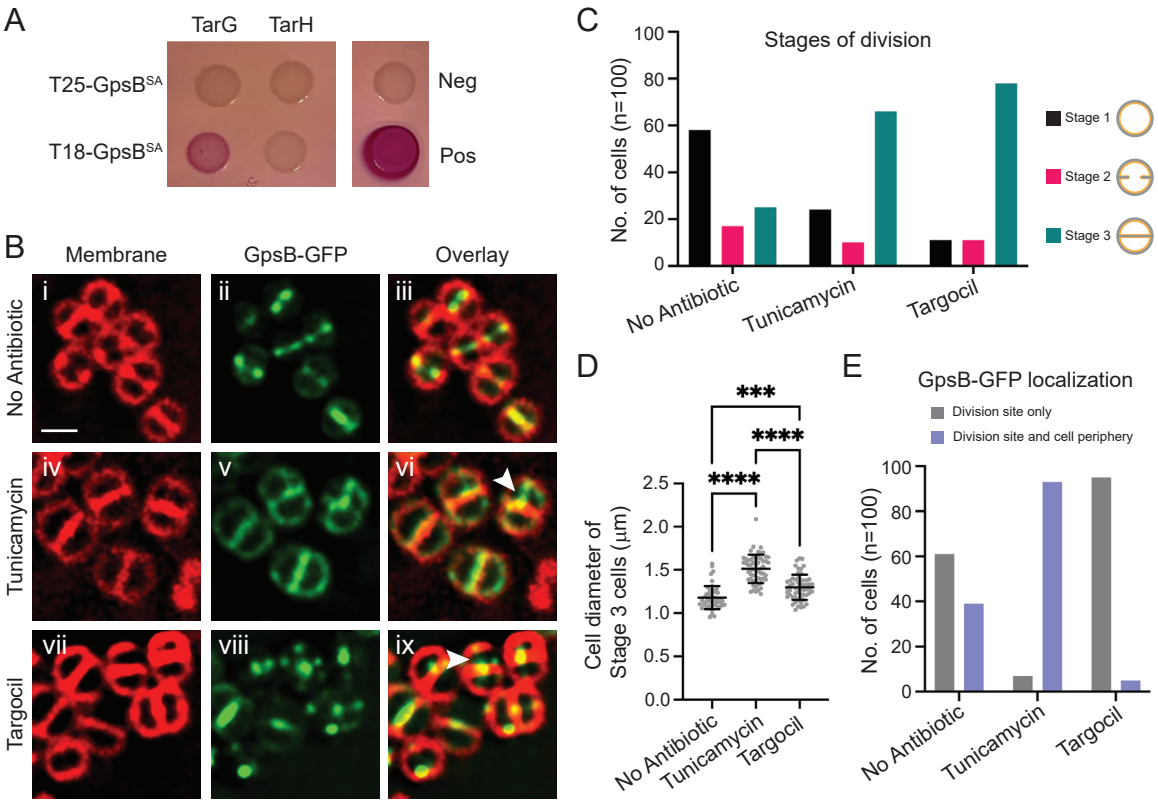

Figure 5

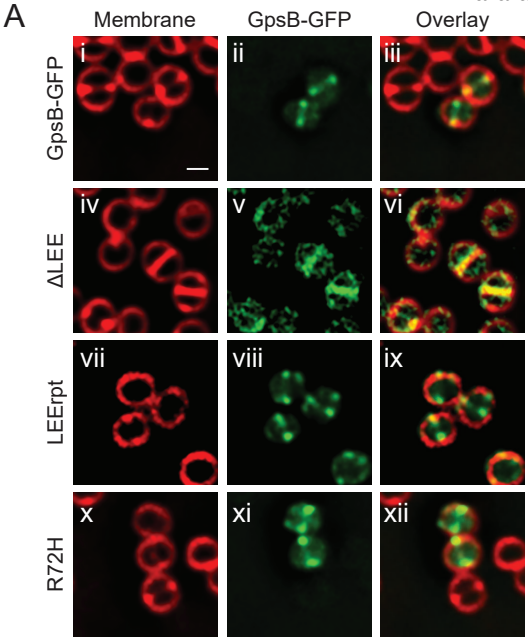

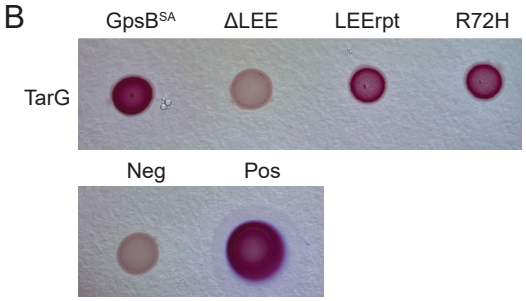

Figure 6

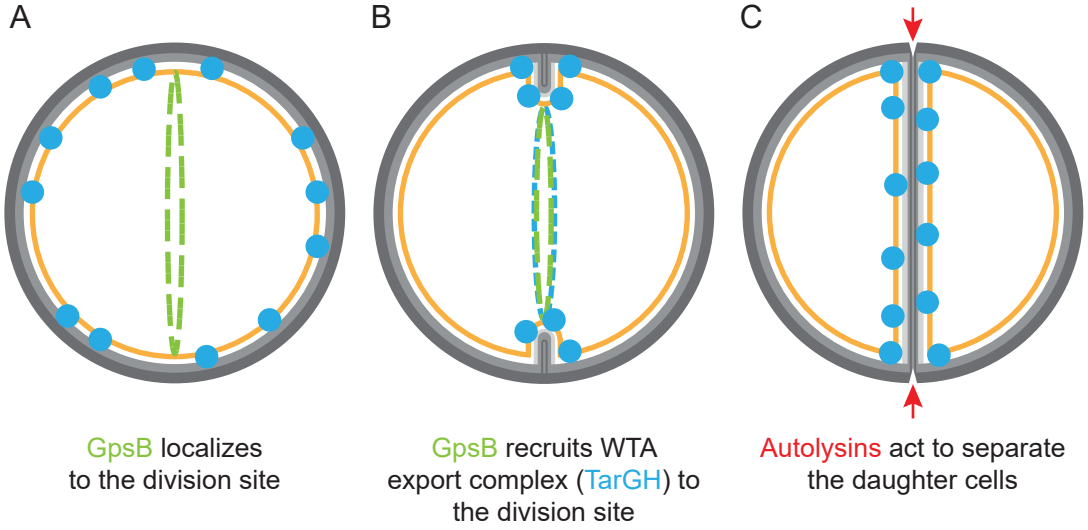

Figure 7